5

Alloying behavior of magnesium and alloy design

M. PEKGULERYUZ, McGill University, Canada

DOI: 10.1533/9780857097293.152

Abstract: Magnesium exhibits significant property improvement via alloying. The addition of thorium to magnesium has to be on the record as leading to one of the highest strengthening responses in a metal. Magnesium alloy research in the past two decades has further shown that magnesium can be designed to improve creep and corrosion resistance and formability. This chapter presents an updated perspective on magnesium alloy design. The solute and second-phase effects of the alloying additions are discussed separately. The spotlight is placed on alloy properties rather than alloying elements. Surface-active elements in magnesium and recent findings on alloy design with respect to wrought texture are highlighted.

Key words: magnesium, alloy design, intermetallics, creep, corrosion, recrystallization, texture, surface-active elements.

5.1 Introduction

The development of magnesium alloys had a golden period in the 1940s and 1950s. Military applications of magnesium led to the development of various magnesium alloys, and the post-war period later led to the use of some of these alloys in civilian applications. Notably, the 1970s VW Beetle and the Super Beetle, the prime user of Mg, featured an air-cooled Mg engine block. In the 1980s cost sensitive industries such as the automotive sector shifted their interest to other materials, mainly steel and cast iron, while the aerospace industry started looking into polymer composites. The 1980s and 1990s may be considered as a dormant period in terms of interest in magnesium.

Since the 1990s, there has been renewed interest in using Mg in weight-sensitive applications. The transport industries have been facing weight reduction objectives to attain fuel economy and high performance in their vehicles since the beginning of the twenty-first century[1–3] and have started to look for materials that are lightweight. At the beginning of that

© Woodhead Publishing Limited, 2013

period, there were really three or four major commercial Mg alloy systems, such as Mg–Al–Zn, Mg–Al, and Mg–Zn–Rare earth (RE) and Mg–RE. In 1990s, most magnesium usage for structural applications was in die-casting (36 kt), and 90% of this was in one alloy, AZ91D (Mg–9wt%Al–1wt%Zn). Later, Mg–Al (AM) casting alloys without Zn were used due to their higher ductility. The RE containing alloys, though used in the aerospace industry, were not readily adopted by car makers due to their high cost.

The beginning of 2000s brought the development of casting alloys with high creep resistance and low-to-moderate cost, for use in powertrain applications. Mg–Al alloys with RE and alkaline earth elements (RE, Ca, Sr) made their debut.[1–3] Magnesium–aluminum–strontium alloy (AJ62), developed by Noranda, was used in BMW engine blocks from 2004 to 2009.[4–6] These activities were not sufficient to develop a steady Mg supplier base, either in North America or in Europe, and, despite the low cost production of Mg in China in the latter part of the decade (2000–2010), wide ranging application of magnesium in the transport industries was not achieved. The new decade from 2010 onward is seeing interest in Mg wrought alloys for use in the automotive body (closures, front-end structure, roof pillars). Extrusion and sheet alloys are currently being developed to improve formability in wrought magnesium. Interestingly, these alloys, like creep-resistant casting alloys, are also based on RE and Sr additions to magnesium.

A lot more research is needed to develop magnesium alloys with improved properties. There is also interest in the use of magnesium in civilian aircraft and in biomedical applications. Mg alloys need to meet the requirements of high ignition resistance or corrosion resistance. This chapter gives an overview of the alloying behavior of magnesium and provides an insight into how certain materials properties can be obtained in magnesium via alloying.

5.2 Alloy design: solid solution alloying of magnesium

Pure metals are rarely used in structural applications. Alloys, which are strengthened via mechanisms such as solid solution strengthening, precipitation hardening and dispersion strengthening (that occur when a metal is combined with one or more elements), form the basis of structural metallic materials. Also, properties of an alloy can be altered and improved via microstructural design and modification.

A solid solution alloy is characterized by the complete dissolution of the alloying element (solute) in the lattice of the base metal (solvent), either substitutionally (substituting the lattice sites of the host) or in the interstitial sites. Mg does not have any major interstitial alloys. According to the

© Woodhead Publishing Limited, 2013

Hume–Rothery rules, extensive solid solutions cannot be formed if the atomic sizes of the solvent and solute differ by more than 15%. In the case of Mg, which has an atomic diameter of 3.2 Å, the elements that fall in this favorable size range are Li, Al, Ti, Cr, Zn, Ge, Yt, Zr, Nb, Mo, Pd, Ag, Cd, In, Sn, Sb, Te, Nd, Hf, W, Re, Os, Pt, Au, Hg, Tl, Pb and Bi.[7–9] Additionally, a metal forms extensive solid solutions with metals of similar electronegativity and crystal structure. Valency also plays a role; a metal of low valency is more likely to dissolve one of higher valency than the reverse (relative valency effect) because the addition of extra electrons to a metal increases its bond-forming capacity and hence the stability of the metal structure. According to this rule, among the elements that have favorable size factors, divalent Mg would dissolve trivalent and higher valency elements in addition to divalent ones. However, as the solute valency increases (groups IV–VII) so does the difference between the electrochemical characteristics of the solute and Mg, which is highly electropositive. In these cases, Mg forms second phases or stable compounds (intermetallic compounds) rather than solid solutions. If these criteria are not satisfied, there are still possibilities for limited solid solutions.

Figure 5.1[7] shows the alloying behavior of Mg with respect to favorable size, relative valency and electronegative valency effects. The elements inside the curve present a group where there is at least a minimum of 0.5 wt% maximum solid solubility in Mg (percentages indicated in parentheses under the element). *In this chapter the alloy compositions are given in weight percent unless otherwise indicated.* The highest solid solubility exists when size factors and relative valency are very favorable (up to 15% relative size, and valency of 2 or 3). In this region, solid solubility can be as high as 53% for In. However, the strengthening effect is not appreciable for these cases, due to extreme similarity of atom sizes. At around 12–15% size factor, where border line sizes are involved, alloy systems of Mg offer considerable solid solution strengthening (Al, Zn, REs, etc.).

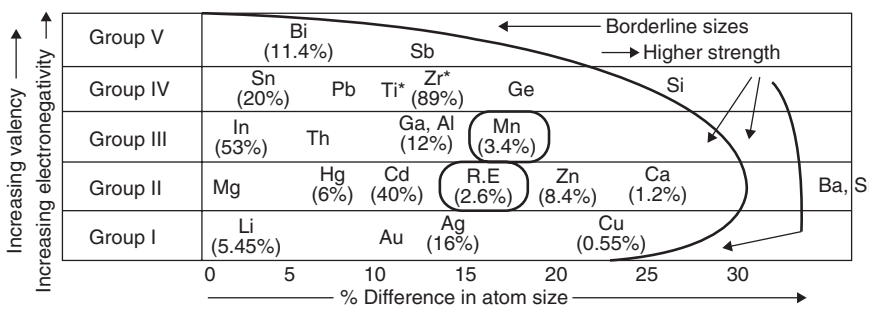

5.1 Alloying behavior of Mg.[7]

© Woodhead Publishing Limited, 2013

5.2.1 Solute hardening

The solute atoms which substitute solvent atoms at lattice sites provide strengthening to the base metal by (i) atom misfit creating elastic lattice strain and (ii) differences in elastic moduli of solute and solvent atoms. Yield strength of the solid solution, σ_y, would increase in proportion to the one-half power of the solute concentration, C. The strengthening is also proportional to the three-halves power of the lattice strain e_s created by the solute; the lattice strain is proportional to the atom radii difference between Mg and the solute:

$$\sigma_y \; \alpha \; \varepsilon_S^{\frac{3}{2}} C^{\frac{1}{2}}$$

where

$$\varepsilon_s \; \alpha \; \Delta r, \quad \Delta r = (r_{\mathrm{Mg}} - r_{\mathrm{solute}}).$$

An additional effect of the solute is its segregation to dislocations, grain and sub-grain boundaries. Solutes can pin dislocations producing solute drag stress, σ_{drag}, which increases the yield strength especially at room and moderate temperatures. Temperature, however, causes unpinning of the solute atmosphere, due to atom diffusion. The effectiveness of the solute pinning at elevated temperatures (>1/3 T_m) depends on solute diffusivity (and hence melting point, T_m). High melting point solutes such as Mn will maintain the effect up to high temperatures, while low melting point Al, Zn, Sn atmospheres around dislocations can be lost at moderate temperatures, leading to the loss of the drag stress.

5.2.2 Other effects of solutes

Solute effects on recrystallization, grain growth and preferred orientation in wrought alloys

Solute pinning can affect the mobility of sub-grain boundaries and grain boundaries, thereby slowing the recrystallization and grain-growth kinetics. Solute pinning of basal dislocations in magnesium can increase the critical resolved shear stress (CRSS) for basal slip, activate non-basal slip at moderate temperatures, and cause texture alteration. A solute effect of Ce has been postulated for Mg–Mn–Ce alloys, which has led to weakened textures after rolling and annealing.[10] This was attributed to a possible change in stacking fault energy (SFE) in another study.[11]

© Woodhead Publishing Limited, 2013

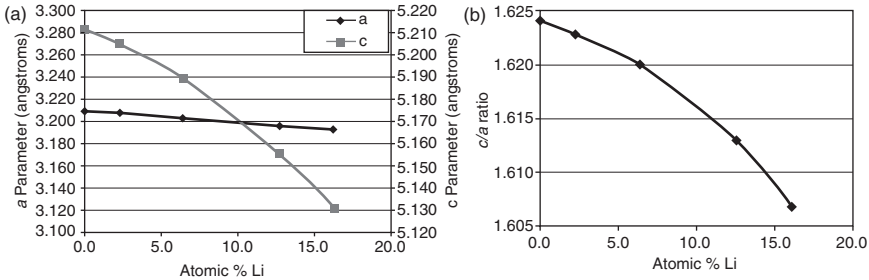

5.2 The effect of Li on the (a) lattice parameters and (b) the axial ratio of Mg.[13]

Axial ratio, deformation, twinning and edge cracking in wrought alloys

Lithium additions above 5.5 wt% change the hexagonal close-packed (HCP) structure of Mg to body-centered cubic (BCC).[8] Small amounts of lithium alloying are also known to improve the room temperature formability of magnesium, which is associated with the activation of non-basal slip with the decrease in the axial ratio (*c*/*a*) of magnesium as a function of lithium.[12,13] As lithium is added to magnesium, the *c* value of the hcp crystal falls faster than the *a* value (Fig. 5.2), which leads to a decrease in the *c*/*a* ratio.[13,14] As a result, the Peierls stress, which is proportional to $e^{-(d/b)}$ where d is the interplanar spacing and b is the Burgers vector (and consequently the CRSS), for basal slip increases relative to that for prismatic slip, and activates slip on non-basal planes. Texture modeling and transmission electron microscopy (TEM) studies indicate that lithium additions also increase the glide of <*c* + *a*> dislocations on {1 1–2 2} pyramidal planes.[11,15] There is evidence that <*c* + *a*> dislocations dissociate into partial dislocations,[16] and lithium may lower the energy of the stacking fault, and thereby increase the stability of the glissile dislocation configuration.[15] Lithium has been observed to alter the crystallographic texture by altering the balance of deformation mechanisms, which in turn influences the texture.[11]

The effect of low levels of Li on the *c*/*a* ratio and grain size of Mg was investigated by Becerra *et al.*[13,17] in Mg–Zn–Li and Mg–Zn–In–Li solid solution alloys. The mono-valent Li decreased the axial ratio (*c*/*a*) of magnesium from 1.624 to 1.6068 within the 0–16 at% Li range (Fig. 5.2). This was attributed to the decrease in *e*/*a* (number of electrons per atom) causing electron overlap from the second Brillouin to the first Brillouin zone; this causes a contraction of the *c*-spacing in real space and a decrease in *c*/*a*. The divalent zinc showed no effect on *c*/*a* in the 0.2–0.7 at% range, since, as explained by Vegard's law, the atom size caused a similar change in both *a*- and *c*-parameters. The trivalent indium increased the *c*/*a* of magnesium

© Woodhead Publishing Limited, 2013

Table 5.1 Axial ratio, grain structure and size, edge cracking index and texture intensity[18]

Alloy, wt%	*a*	*c/a*	Effective cast grain size *D′*, mm	Recrystallized grain size, *d*, μm	Edge cracking index	Maximum Intensity	
						Roll	Roll + anneal
Mg	3.2088	1.6240	6.1	46	High/4	12.2	17.9
Mg–1.8Li–1Zn	3.2009	1.6190	1.8	48	Minimum/1	4.2	2.6
Mg–6Li–0.4Zn–0.2In	3.1991	1.6190	1.0	49	Minimum/1	6.2	3.0

*D_c = average diameter of columnar grains = $(D_{minor} + D_{major})/2$; D = average grain diameter of equiaxed region.

to 1.6261 as In increased towards 3.3 at%. An important effect of *c/a* was seen (Table 5.1) in the twinning behavior of the alloys and in turn on edge cracking during 150°C rolling.[18]

The changes in axial ratio and lattice parameters influence slip systems and twinning modes in HCP metals. The change in the deformation mechanism with reduced axial ratio can be attributed to the change in interplanar spacing, *d*, since the shear stress required to move dislocations is given by the Peierls stress,

$$\tau_\pi = \mathrm{P.\ e}^{\{-2s\ d/[b(1-\nu)]\}}, \qquad [5.1]$$

where P is a factor depending on the shear modulus and Poisson's ratio, ν; b is the magnitude of Burgers vector of the dislocation; and d is the interplanar spacing. The CRSS, τ_{CRSS}, is related to the Peierls stresses, τ_p. In a recent study, Uesugi *et al.*[19] have calculated τ_p from first principles as

$$\tau_p = \frac{Kb}{a'} \exp\left(-\frac{Kb}{2a'\tau\max}\right), \qquad [5.2]$$

where K is the energy factor (depending on elastic constants and the type of dislocation); a' is interplanar spacing in the direction of dislocation sliding on the slip plane ($a' = a/2$ for basal slip where a is the lattice parameter and $a' = a$ for prismatic plane); b = Burgers vector; $b = (a/3)^{1/2}$ for Shockley partial dislocations of the basal plane and $b = a$ for edge dislocations of the prismatic plane; τ_{max} is the maximum restoring force (= maximum slope of the generalized SFE in the analysis). Equation [5.2] interestingly indicates that changing the a-spacing would not influence the Peierls stresses and CRSS for prismatic slip (because $b = 2a$ for edge dislocations), but it would alter the basal slip of partial dislocations because their $b = (a/3)^{1/2}$.

© Woodhead Publishing Limited, 2013

Effects of cast grain size were seen on the texture evolution of Mg alloys.[18] The 150°C rolling produced deformation structures and texture, and static recrystallization occurred during post-annealing. Maximum texture intensity during 150°C rolling and subsequent annealing correlated strongly with the cast grain size (Table 5.1). The texture weakened with decreasing grain size, which was attributed to the activation of non-basal slip by plastic compatibility stresses at grain boundaries. The *a* lattice parameter exerted a weaker influence on texture, possibly by facilitating the cross-slip of partial dislocations at grain boundaries.

The other important effect of *c*/*a* is on the twinning behavior of Mg. The twinning shear is related to the axial ratio in HCP crystals[20–22] as presented in Fig. 5.3, where the twinning systems with positive slope indicate compression (contraction) twins and those with negative slopes indicate tension (extension) twins along the *c*-axis. Figure 5.3 also presents the axial ratios of the HCP metals and the most common twinning modes activated in them. Within the range of the axial ratios of the HCP metals (1.568–1.886), the {10–12}<–1011> shear direction reverses at a *c*/*a* of $\sqrt{3}$, where this twinning mode becomes compressive for Zn and Cd, but is tensile for all other HCP metals (Be, Ti, Zr, Re, Mg). HCP metals that exhibit high ductility (Re, Zr, Ti) twin profusely in both tensile and compressive modes and those that are very brittle (Be, Zn) twin only by the most common type {10–12} tension twin.[20] In Mg, the {10–12} tension twins are followed by {10–11} compression twins. Generally, the lower the value of twinning shear of a given twin mode, the higher is the frequency of its occurrence. This correlation has been generally observed as indicated by Fig. 5.3 and also by those experiments in which the axial ratio was changed by alloying;[20] the additional factors are the ease with which atomic shuffling can occur to nucleate the twin and the ease of gliding parameters. The absence of {10–11}[10–12] compression twins in Be, despite the low twinning shear, is related to the complex atom shuffling, while the occurrence of {11–21} 1/3 [–1–126] twinning in Ti, Zr and Re in spite of its relatively large twinning shear is attributed to the relatively simple atomic shuffling.[20] It has been observed that subsequent slip-twin interactions largely determine the ductility of the HCP metals that undergo twinning.[20] If the twin boundaries become sinks for gliding dislocations the metal is ductile; if however, the dislocations are repelled by the twin boundary they pile up at the interface leading to eventual crack nucleation. In Mg, the basal dislocations are repelled by {10–12} tension twins[20] leading to edge cracking. It is known that the twinning modes in HCP metals are altered via alloying[20] that changes the axial ratio; for example, twinning is stopped in Mg–Cd alloy with $c/a = \sqrt{3}$, leading to extreme brittleness. It is, therefore, possible to influence the twinning behavior of Mg alloys via changes in *c*/*a*.

In the study by Pekguleryuz *et al.*,[18] the differences in the twinning modes of Mg–3Al–1Zn (AZ31) and Mg–2Li–1Zn and Mg–6Li–0.4Zn–0.2In,

© Woodhead Publishing Limited, 2013

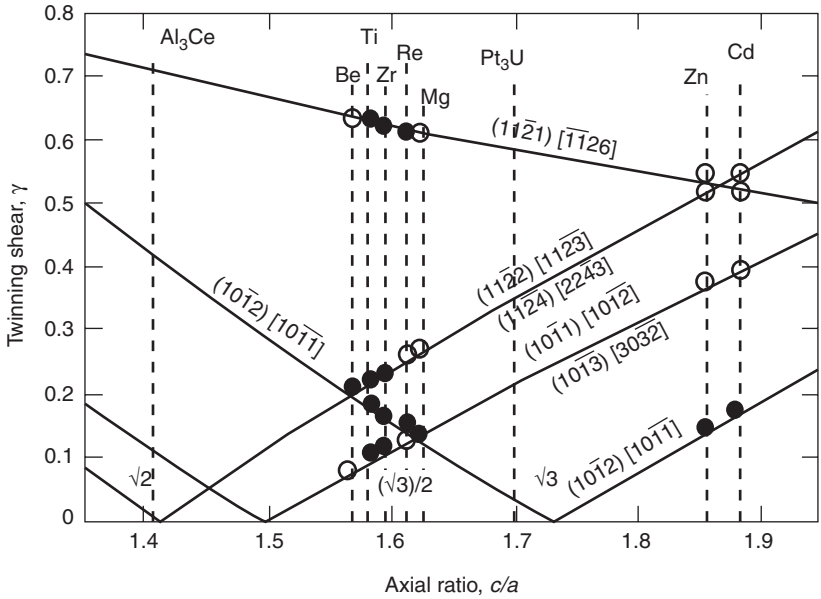

5.3 Twinning shear versus axial ratio in HCP metals.

which governed the edge cracking index (Ic) during 150°C rolling, have been related to the axial ratio. AZ31 alloy significantly edge-cracked during rolling, twinned in the tensile mode, and had a *c*/*a* (axial ratio) of 1.6247. At the *c*/*a* of 1.6247, the shears of {10–12} tension twins and {10–11} compression twins start to differ, making the atomic reshuffling more difficult, impeding double twinning in AZ31, and leaving a higher propensity of tension twins which are potent sites for crack nucleation. The Li-containing alloys (Mg–2Li–1Zn and Mg–6Li–0.4Zn–0.2In) had lower *c*/*a* (Table 5.1), double-twinned during rolling, exhibited a lower degree of twin-related brittleness and did not edge-crack during rolling.

Solute effects on creep

Creep resistance can be improved via solid solution if the solute can (i) decrease the homologous temperature, (ii) increase the elastic modulus or (iii) decrease diffusivity as proposed by Sherby[23] via

$$\varepsilon = S\left(\frac{\sigma}{E}\right)^{\eta} D \qquad [5.3]$$

where ε is steady-state creep rate, S is a structure term (grain morphology, dislocation density, distribution, etc.), σ is stress, E is elastic modulus, D is self-diffusivity and η is the stress exponent.

© Woodhead Publishing Limited, 2013

While most creep-resistant alloy-development work in the 1990s and 2000s focused on ternary additions to Mg–Al based alloys that can suppress creep-induced $Mg_{17}Al_{12}$ precipitation, one alloy family, Mg–RE–Zn, has re-explored the effects of REs on Mg–Zn alloys.[24,25] Zhu *et al*.[25] studied the addition of different RE elements (La-rich and Nd-rich) in Mg–2.5RE-0.6Zn alloys. They found that the primary creep (which is a competition between work hardening and work softening) was more extensive in the La-containing alloy, but there was no discernible difference in the steady-state creep rates of the two alloys. The authors related the difference in the primary creep of the two alloys to the higher solid solubility of Nd than that of La in Mg. The higher solubility can indeed provide a richer solute atmosphere around the dislocations, increasing work hardening in the Nd-alloy.

Mg alloys with Ce-based REs have been further developed into ternary compositions with low level additions of Mn. Mn was found to improve the creep resistance of Mg–Ce alloys by increasing the solid solubility of Ce in Mg at high temperatures. The work carried out in Germany before World War II showed that Mg–6RE–2Mn alloy has good creep resistance (300–315°C, ~ 14 MPa). Mg–2RE–1Mn alloy was observed to be much stronger at elevated temperatures than any of the cast Mn-free alloys.[8] Mg–2.25RE–0.5Mn and Mg–2RE–1.25Mn–0.2Ni alloys were also creep-resistant compositions.[26]

Diffusional creep can occur at relatively low temperatures (~0.4 T_m) when the stresses are high through diffusion along dislocation cores, which is called *pipe diffusion*. Solutes which segregate to dislocations can impede *pipe diffusion*. These should conceivably be solutes with significant difference in metallic radii so that enhanced segregation to dislocations can occur. However, at higher temperatures solutes in the dislocation atmosphere become mobile and dissociate from the dislocations, therefore, for high temperature service, high melting point solutes with lower diffusivity need to be selected.

Pipe diffusion has not been considered in many of the creep studies carried out on magnesium alloys. AZ91D alloy at stresses above 50MPa in the 125–175°C range gave an n value of 5 and Q value of 94 kJ/mole, which can be related to pipe diffusion.[27] AJ63 alloy also gave an activation energy, Q, of 92 kJ/mol at 50 MPa in the 150–200°C range, which can also be related to pipe diffusion.[6] In AJ63 the grain boundaries are stronger than AJ62, due to the higher amount of intermetallics, and the dislocation cores, in that case, would become more open to diffusion than the grain boundaries. Recently, Mg–Mn–Sr was found to be susceptible to *pipe diffusion* at moderate temperatures,[28] basically due to the low solubility of Sr in Mg. Age-hardened Mg–Gd–Nd–Zr at 250°C/50 MPa exhibited Q of 109 kJ/mol, where pipe diffusion can also be a possible mechanism.[29] These alloys would benefit from the addition of high temperature solutes with adequate solubility for impeding creep deformation related to pipe diffusion.

© Woodhead Publishing Limited, 2013

5.3 Alloy design: compound formation in magnesium alloys

When the Hume–Rothery rules for solid solution formation do not hold, compound formation occurs. Second phases are important in strength, creep resistance, and recrystallization and texture. Important intermetallic compounds found in Mg alloys are listed in Table 5.2,[30] some of which are described in some detail below.

5.3.1 $Mg_{17}Al_{12}$

The $Mg_{17}Al_{12}$ intermetallic phase has a cubic A12 crystal structure isomorphous with α-Mn (cI58) with the space group of $I43m$ (Table 5.2, Fig. 5.4) and lattice parameter a = 1.06 nm. The unit cell contains 34 Mg atoms and 24 Al atoms. The unit cell has the highest symmetry T_d^3 and its atomic coordinates are shown in Fig. 5.4.[31]

It has been explained[8] that Al–Al bonds are homopolar, each Al atom accepting an electron from the structure as a whole from the 24 Mg nearest neighbors, while the other ten Mg atoms retain their valency electrons. The structure is designated as twelve (12) Al pairs of two negative charges, twenty-four (24) positively charged Mg atoms and ten (10) Mg atoms in their normal state: $(Al_2)_{12}^{-2}Mg_{24}^{+}Mg_{10}$. The structure is interesting in that in one intermetallic compound both homopolar, heteropolar and normal metallic characteristics are present.[8] The planes (033)p and (411)p are both identified as close-packed planes, but there is also (877)p, which exhibits lower diffraction intensity but its d spacing is one-third of the d spacing of (033)p or (411)p, that is, 0.8289 Å.[32] The $Mg_{17}Al_{12}$ phase has also been reported with 44.5 at%Mg with a tetragonal structure of a = 10.50 nm, c = 10.19 nm.

The γ-$Mg_{17}Al_{12}$ is the main second phase[33] which forms eutectically in Mg–Al alloys and also in Mg–Al–Zn alloys with high Al:Zn ratio (Fig. 5.5a).

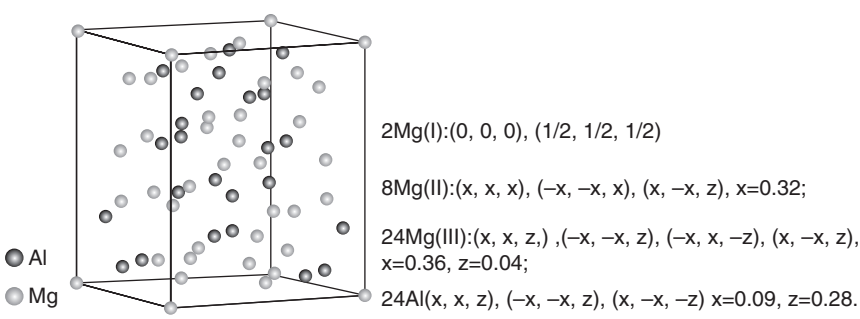

5.4 The crystal structure of $Mg_{17}Al_{12}$.[31]

© Woodhead Publishing Limited, 2013

Table 5.2 The crystal structure data of important equilibrium intermetallic phases in Mg alloys

Phase	Melting point (°C)	Crystal structure	Pearson symbol	Space group	Lattice parameters		
					a (nm)	*c* (nm)	*c*/*a* or *b**
$Mg_{17}Al_{12}$	450	Cubic A12	cI58	$I\bar{4}3m$	1.06	–	–
		Tetragonal	–	–	1.05	1.02	0.97
Mg_2Ca	714	Hexagonal C14	hP12	*P63/mmc*	0.62	1.02	
Al_2Ca	1079	Cubic C15	cF24	*Fd3m*	0.80	–	
$Al_2(Mg,Ca)$		Hexagonal C14	hP12	*P63/mmc*	0.56	0.90	1.6
		Hexagonal C36	hP24	*P63/mmc*	0.55	1.75	3.2
Mg_2Si	1081	Cubic C1	cF12	$Fm\bar{3}\ m$	0.63	–	–
$Mg_{12}Ce$	616	Tetragonal	tI26	*I4/mmm*	1.03	0.60	0.58
$Mg_{12}Nd$	548	Tetragonal	tI26	*I4/mmm*	1.03	0.59	0.57
B-$Mg_{14}Nd_2Y$		Cubic A12	cI58	$F\bar{4}3m$	2.2		
B_1-$Mg_{12}NdY$		Cubic C1	cF12	$Fm\bar{3}\ m$	0.74		
$Al_{11}RE_3$	1020†	Tetragonal	tI26	*I4/mmm*	0.44	1.01	2.30
		Orthorhombic	oI28	*Immm*			1.30*
Al_2RE	1455,1480	Cubic	cF24	*Fd3mS*	0.81		
$Mg_{17}Sr_2$	606	Hexagonal	hP38	*P63/mmc*	1.05	1.03	0.98
Al_4Sr	1040	Tetragonal	tI10	*I4/mmm*	0.44	1.11	2.52
$Mg_{24}Y_5$	567	Cubic A12	cI58	$I\bar{4}3m$	1.13	–	

*The value is for parameter *b* rather than *c*/*a*.
†Transformation *T*.

In non-equilibrium solidification, the α-Mg matrix becomes supersaturated in Al, especially in the interdendritic regions which give rise to the discontinuous precipitation of $Mg_{17}Al_{12}$ (γ_d in Fig. 5.5a) when exposed to elevated temperatures. The alloys can be heat-treated by dissolving the γ-phase through long (24 h) solution treatment and re-precipitating it as a discontinuous fine plate-like phase (Fig. 5.5b and 5.5c).

Six different orientation relationships (OR) are found in the Mg/γ-$Mg_{17}Al_{12}$ precipitation system.[127,128] The initial lattice correspondence between HCP and BCC structures (Fig. 5.6a and 5.6b) is described by the Pitsch–Schrader OR,[34] as shown in Fig. 5.6c: The Pitsch–Schrader OR requires that the close-packed planes in the BCC lattice should be parallel to the close-packed planes or near-close-packed planes in the HCP lattice, that is, (011)p // (0001)m and (011)p // (0110)m. Multiple morphologies, growth directions and habit planes are described as twining versions of the initial Pitsch–Schrader OR.

γ-$Mg_{17}Al_{12}$ is an intermetallic that has a composition range (Table 5.2). It strengthens Mg–Al alloys and the AZ91; however, it is also prone to deformation by slip. The γ phase increases the strength by creating obstacles to slip and accumulating dislocation pile-up at its interface up to a certain level of strain (2.1%); however, further strain (5.4%) does not change the

© Woodhead Publishing Limited, 2013

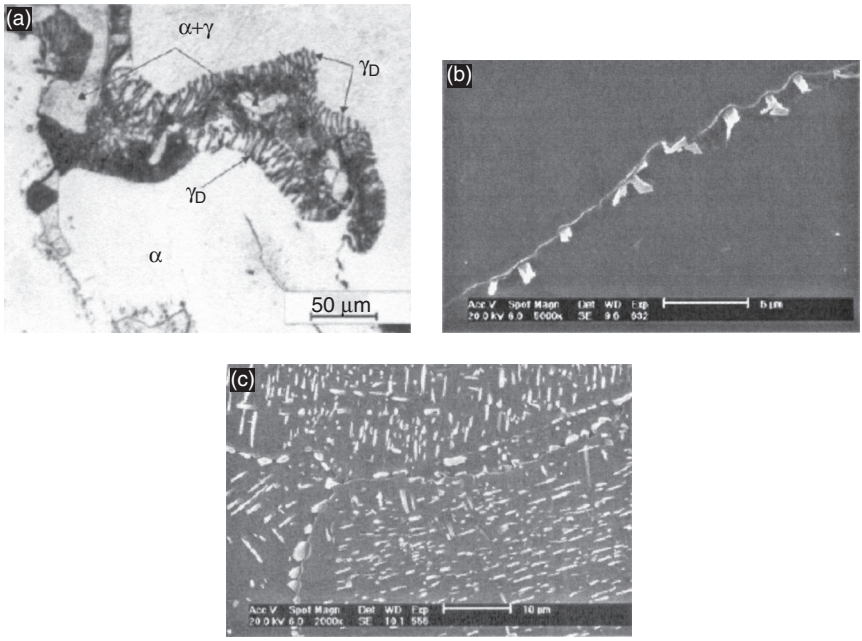

5.5 (a) Eutectic γ-$Mg_{17}Al_{12}$ precipitates and discontinuous γ_d-$Mg_{17}Al_{12}$ precipitates in AZ91. (b) Grain boundary γ-$Mg_{17}Al_{12}$ precipitates and (c) discontinuous γ_d-$Mg_{17}Al_{12}$ precipitates in AZ91 alloy after aging at 623 K; SEM.[33]

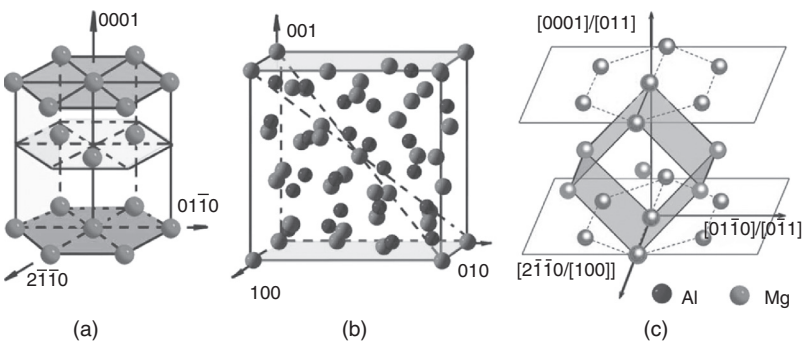

5.6 The crystal structures of the two phases in the transformation system Mg/γ-$Mg_{17}Al_{12}$: (a) HCP Mg; (b) BCC γ-$Mg_{17}Al_{12}$. (c) Schematic diagram showing the initial lattice correspondence between HCP and BCC structures, described as the Pitsch–Schrader OR.[33]

dislocation pile-up, but instead leads to dislocation accumulation inside the γ-phase (Fig. 5.7).[35]

The γ-phase softens at elevated temperatures, due to its partial metallic bonding, which adversely affects elevated temperature strength and creep

© Woodhead Publishing Limited, 2013

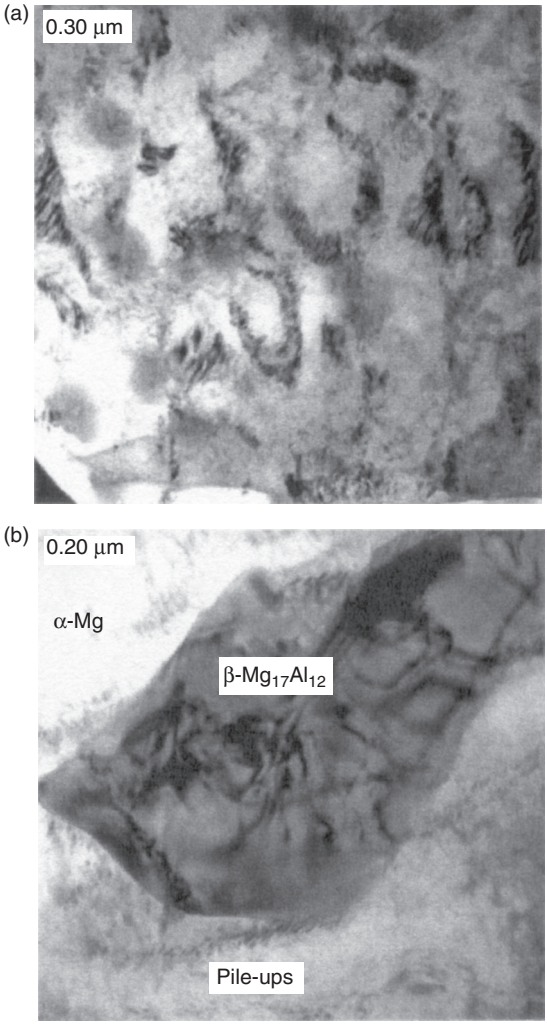

5.7 Dislocation arrangements in AZ91D alloy. (a) Dislocation pile-up after 2.1% deformation, (b) dislocations in the γ-$Mg_{17}Al_{12}$ phase.[35]

resistance. Its discontinuous precipitation from the supersaturated α-Mg matrix during creep leads to grain boundary deformation and migration. Many alloys have been developed to improve the creep resistance by adding Ca, Sr and REs to Mg–Al alloys to eliminate the discontinuous precipitation of $Mg_{17}Al_{12}$.

Zhou *et al.*[36] have conducted a first principles study to determine the structural stability of Ca alloying of the $Mg_{17}Al_{12}$ phase, and have concluded that the cohesive energy of $(Mg_{17-x}Ca_x)Al_{12}$ (x = 0, 1, 4, 12) phases

© Woodhead Publishing Limited, 2013

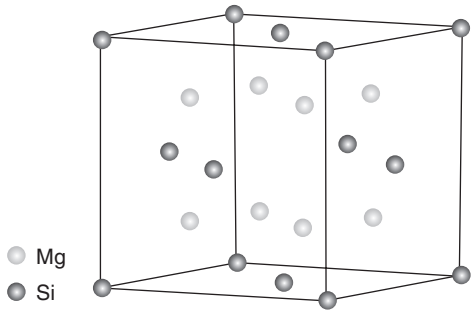

5.8 Mg_2Si unit cell.[37]

gradually increase when Mg atoms in I, II, III positions of $Mg_{17}Al_{12}$ phase are substituted by Ca. Their results have indicated that the $(Mg_5Ca_{12})Al_{12}$ with Ca substitution of the Mg(III) atoms has the highest alloying ability and the highest structural stability.

5.3.2 Mg_2Si

Mg_2Si crystallizes in an FCC (cubic C1) lattice with lattice parameter a = 6.339 Å (Fig. 5.8 and Table 5.2) and with 12 atoms per unit cell. Si atoms are located on the corners and surface centers of the face-centered cubic and Mg atoms are in the eight tetrahedral interstices of the crystal cell. The Mg_2Si has high thermal and mechanical stability.[38] It occurs as a eutectic precipitate in Mg–Al–Si alloys (AS41, AS31, AS21), in addition to the $Mg_{17}Al_{12}$ phase (Fig. 5.9), and renders slight improvement in creep resistance.[39] The morphology is coarse Chinese script when the alloy is cast at slow to moderate solidification rates. High solidification rates, as in high-pressure die-casting, refine the Mg_2Si into polygonal dispersed particles, leading to improved mechanical properties.[40] Trace levels of Ca, Sb, Sr[41–43] also modify and refine to different extent the Mg_2Si morphology (Fig. 5.10).

5.3.3 Intermetallics with Ce

$Mg_{12}Ce$

Two crystal structures have been previously reported for $Mg_{12}Ce$: a tetragonal structure ($ThMn_{12}$-type) below the eutectic temperature, and an ordered structure above the eutectic.[44,45] Figure 5.11a shows the unit cell of $Mg_{12}Ce$ with the $ThMn_{12}$ tetragonal (Pearson symbol tI26) structure,[46] which has two (2) cerium and twenty-four (24) magnesium atoms with all the cerium atoms at the 2a position, and magnesium atoms occupying the 8f, 8i and 8j

© Woodhead Publishing Limited, 2013

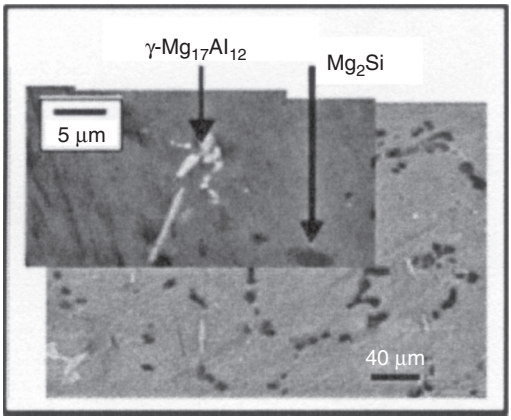

5.9 SEM image showing Mg_2Si and γ-$Mg_{17}Al_{12}$ precipitates in AS alloys.[39]

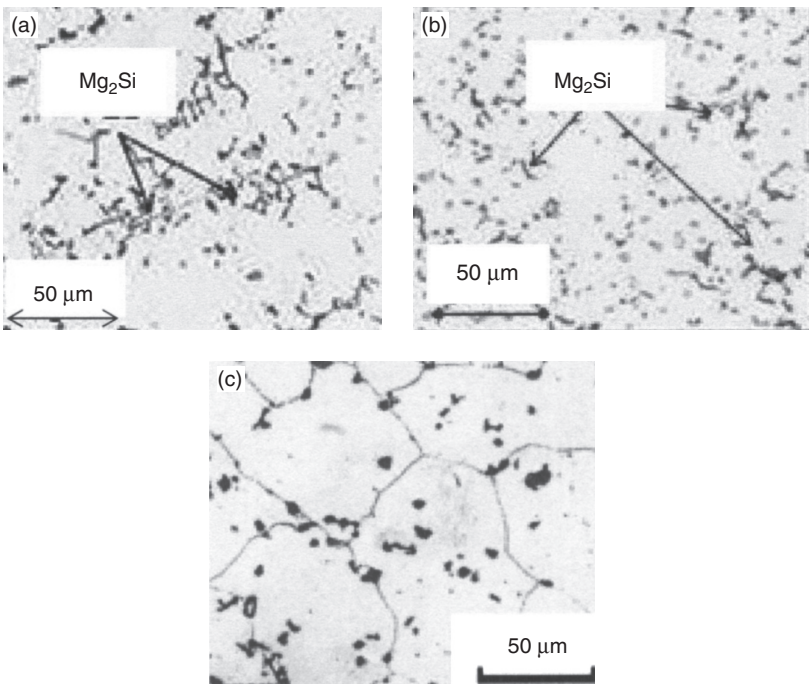

5.10 Microstructure of gravity cast (a) AS41 alloy with Chinese script Mg_2Si phase; (b) same alloy with 0.1 wt% Ca with refined Mg_2Si phase.[41] (c) Heat-treated AZS511 with 0.5 wt%Sb with fine Mg_2Si.[42]

© Woodhead Publishing Limited, 2013

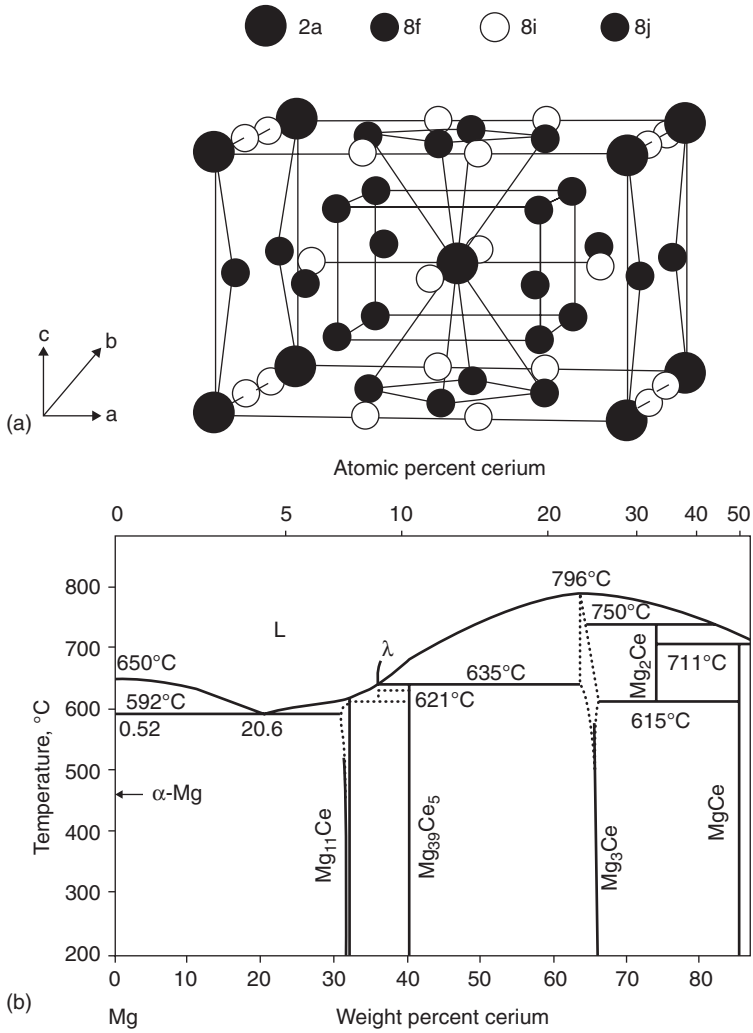

5.11 (a) Unit cell of the ThMn12 type structure.[46] (b) Revised Mg–Ce phase diagram up to 50 at% Ce.[48]

positions. The coordination number is 12. In the phase diagram (Fig. 5.11b) of the Mg–Ce binary system,[4] a dotted line to the left of $Mg_{12}Ce$, shows a small compositional range, which increases when the temperature increases above ~450°C.[4]

Xin *et al.*[46–48] have made an in depth study of the $Mg_{12}Ce$ along with the other Mg–Ce intermetallics in the binary phase diagram up to 50 at%Ce and have concluded the intermetallic in the region of 8–10 at%Ce to be a vacancy defect structure of $Mg_{12}Ce$ with the real composition of $Mg_{11}Ce$ and suggested the phase diagram shown in Fig. 5.11b.

© Woodhead Publishing Limited, 2013

Magnesium alloys containing Ce, which are commercially available, usually contain Zn, and/or Mn as well; in these alloys the β-$Mg_{12}Ce$ exists as a second-phase precipitate but exhibits solubility for Mn or Zn. Xin *et al.*[49] have made EPMA studies of the $(Mg, Mn)_{12}Ce$ in Mg–Ce–Mn alloys and have determined ~0.8 at% Mn in the intermetallic. Moreno *et al.*,[50] have observed 0.07 at% Mn and 1.2 at%Zn in the $(Mg,Zn)_{12}Ce$ of the MEZ alloy. These observations fit well with the vacancy defect structure of the $Mg_{12}Ce$. The Mn solubility of $Mg_{12}Ce$ has an important influence on the creep behavior of Mg–Ce–Mn alloys.[51] The dynamic precipitation of nano-particles of Mn from the intergranular $(Mg, Mn)_{12}Ce$ phases provides effective dislocation pinning in the grain boundary regions and prevents the local recovery phenomenon in the vicinity of the intermetallics. This local recovery involves the formation of high dislocation density (HDD) zones next to dislocation-free zones at the intermetallic/matrix interface, which lead to stress accumulation at the HDD zones and subsequently cracking of the intermetallic. The dynamic precipitation of nano-sized $Mg_{12}Ce$ dispersed inside the α-Mg grains is also observed during the creep of Mg–Ce–Mn alloys, a phenomenon due to the Ce supersaturation of the α-Mg. These particles improve the creep resistance by effective dislocation pinning.

$Al_{11}RE_3$ and Al_2RE

The $Al_{11}Re_3$ intermetallic has the tetragonal structure with the space group I4/mmm and lattice parameters $a = 4.365$, $b = 4.365$ and $c = 10.10$. Its melting point is 1235°C. The Al_2RE has cubic with the Fd3mS space group; its melting point is 1200°C. These intermetallics exist in the interdendritic regions of Mg–Al–RE alloys (e.g., AE42, AE44). In the AE42 alloy, the $Al_{11}RE_3$ that is present in the as-cast alloy is found to decompose when heated above 175°C into Al_2RE and $Mg_{17}Al_{12}$.[52] In the AE44 both intermetallics are present in the as-solidified alloy (Fig. 5.12).[53]

Pettersen *et al.*[54] suggested that when RE/Al weight ratio is above 1.4, all the Al is tied up as $Al_{11}RE_3$, in which case further precipitation of other phases such as another type of Al–RE phase or $Mg_{12}RE$ becomes possible. In samples produced by cold chamber die-casting, $Al_{11}RE_3$ and $Al_{10}RE_2Mn_7$ were observed. The TEM investigation has revealed that the major phase was $Al_{11}RE_3$ (a body-centered orthorhombic cell with lattice parameters a = 4.5 Å, b = 13.2 Å and c = 9.9 Å). The relative amounts of REs were reported to be (at%) $La_{27\pm2}Ce_{51\pm2}Pr_{6\pm1}Nd_{16\pm1}$.This phase co-existed with a minor phase $Al_{10}RE_2Mn_7$, the diffraction patterns of which were indexed to a hexagonal system with lattice parameters a = 9.0 Å and c = 13.1 Å. The relative compositions of the RE components was $La_{10\pm1}Ce_{50\pm3}Pr_{9\pm1}Nd_{31\pm2}$. La was said to go into the $Al_{11}RE_3$ phase, while Nd went into the $Al_{10}RE_2Mn_7$ phase. It must be noted

© Woodhead Publishing Limited, 2013

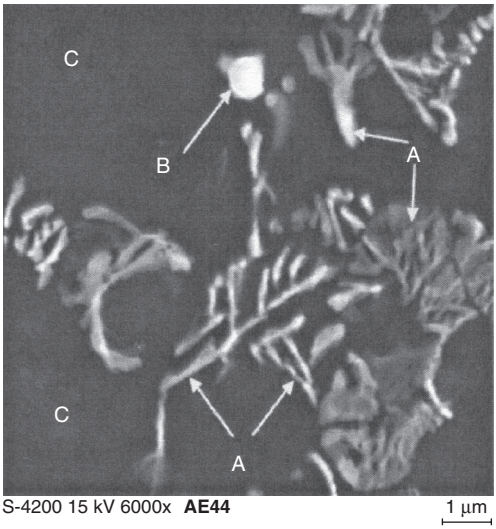

5.12 SEM image of die-cast AE44. Labels A: $Al_{11}RE_3$; B: Al_2RE; C: α-Mg.[53]

that the fast solidification rate of the die-casting process may have influenced the compositions and the crystal structures observed in these studies.

5.3.4 Intermetallics of Ca

In Mg–Al–Ca based alloys, Mg_2Ca and/or Al_2Ca phases are known to form in the interdendritic region in preference to the $Mg_{17}Al_{12}$ phase observed in the binary system. Mg_2Ca and Al_2Ca are Laves phases with crystal structures of C14 (hexagonal) and C15 (cubic), respectively. Al_2Ca and Mg_2Ca, have melting points of 1079°C and 714°C, respectively.[55–57] Mg–Al–Ca alloys also exhibit ternary intermetallics, which has been the topic of much research in order to understand if these are stable or metastable structures.[55,58–62]

Mg_2Ca

Mg_2Ca has a hexagonal C14 type structure with 12 atoms in a unit cell (Fig. 5.13). The lattice parameters are a = 6.2386 Å and c = 10.146 Å and atomic coordinates in the unit cell are shown in Fig. 5.13.[63]

Most of the atoms in the Mg_2Ca unit cell can be classified into two groups. The first group is composed of Ca and Mg(I) atoms, and the second is laid by Mg(II)atoms parallel to each other. The connection between the Ca–Ca–Mg(I) atom group and Mg(II) atom layers depends on three kinds of relatively weak bonds – B, D and F. This indicates that

© Woodhead Publishing Limited, 2013

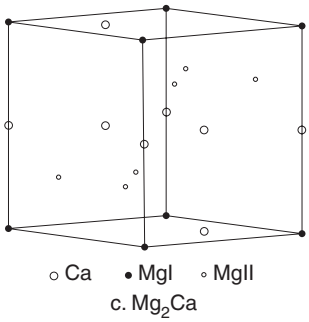

4Ca : $\pm(\frac{1}{3},\frac{2}{3},z;\ \frac{1}{3},\frac{2}{3},-z)$; $z = 0.062$

2Mg(I) : $(0,0,0;\ 0,0,\frac{1}{2})$

6Mg(II) : $\pm(x,2x,\frac{1}{4};\ \overline{2x},\bar{x},\frac{1}{4};\ x,\bar{x},\frac{1}{4})$; $x = -0.170$

5.13 The crystal structure of Mg_2Ca.

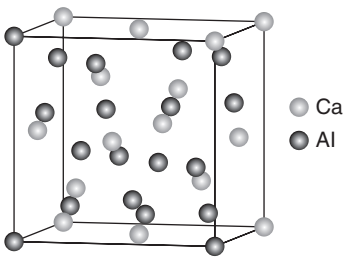

+2Ca: (0,0,0), (1/2,1/2,1/2);

+4Al(I): (0,0,z), (0,0,–z) z = 0.380;

+4Al(II):(0,1/2,1/4),(1/2,0,1/4).

5.14 The crystal structure of Al_2Ca.

the stability of the Mg_2Ca compound is controlled by these weak bonds. When the temperature increases, the expansion of the lattice of Ma_2Ca will produce stress on the bonds connecting atoms. Because the networks of Ca–Ca–Mg(I) and Mg(II)–Mg(II) are so solid and difficult to elongate that the lattice will break on the weak bonds. The existence of the weak bond zones in the Mg_2Ca intermetallic structure is the main reason for its low stability.

Al_2Ca

Al_2Ca has an ordered cubic C15 structure with lattice constants $a = b = c =$ 8.020 Å. As shown in Fig. 5.13; its unit cell has the highest symmetry O_h^T, space group Fd3m. In a unit cell of the Al_2Ca phase, there are 24 atoms and their atomic coordinates are as shown in Fig. 5.14.

Mg–Al–Ca intermetallics

The possible existence of a Laves phase with C36 structure in the pseudo-binary system Mg_2Ca–Al_2Ca was shown by Ameroun *et al.*[56] who carried out first principles calculations and neutron diffraction (ND) analysis on 700°C-annealed samples. The authors showed that the structural sequence in the $CaAl_{2-x}Mg_x$

© Woodhead Publishing Limited, 2013

system is C15–$MgZn_{2(cubic)}$ → C36–$MgNi_{2(hexagonal)}$ → C14–$MgCu_{2(hexagonal)}$. The electron/atom ratio (*e*/*a*) was seen to govern the structural sequence: C15–$CaAl_2$ (cubic) structure is stable above *e*/*a* of 7.75 and until the composition of $CaAl_{1.76}Mg_{0.24}$. The hexagonal C14 is stable below the *e*/*a* value of 6.5 and above the composition of $CaAl_{0.49}Mg_{1.51}$. The C36–$CaAl_{2-x}Mg_x$, structure is stable in the composition range of $0.66 < x < 1.073$. Zhong *et al.*[57] made first principles calculations of three Laves phase structures at Al_2Ca and Al_2Mg compositions and have predicted the existence of various Laves phases in the Al_2Mg and Al_2Ca compositions. Their diffusion couple studies found the existence of two ternary $Al_2(Mg,Ca)$ with C14 (a = 5.56 Å, c = 9.02 Å) and C36 (a = 5.45 Å, c = 17.51 Å) structures via TEM and Orientation Imaging Microscopy (OIM), respectively. The existence of two Laves phases was attributed to the very small energy difference between the Laves phase structures. Based on the explanations of Ameroun,[56] their existence may also be due to a mere change in *e*/*a* ratio with change in composition.

5.3.5 Intermetallics of Sr

Mg–Sr alloys are a new class of advanced Mg alloys; Mg–Al–Sr compositions have been developed as creep-resistant cast alloys[64–68] and Mg–Mn–Sr alloys have been recently investigated for creep resistance.[69] Mg–Sr based wrought alloys are also being currently being investigated.[70–77]

Al_4Sr and $Mg_{13}Al_3Sr$ or Mg_9Al_3Sr

Sr added to an Mg–Al system leads to the precipitation of Al_4Sr phase (Fig. 5.15). Mg–Al–Sr ternary compound formation is also observed in certain Mg–Al–Sr alloys (e.g., AJ52). The Sr/Al ratio seems to determine the phase selection: if the ratio is below 0.3 only Al_4Sr is seen, otherwise a ternary phase ($Mg_{13}Al_3Sr$ or Mg_9Al_3Sr) precipitates.

$Mg_{17}Sr_2$

$Mg_{17}Sr_2$ is the most Mg–rich stable compound in the Mg–Sr system. It has the $Ni_{17}Th_2$-type hP38 hexagonal structure. It forms in Mg–Sr alloys not containing Al,[69–72] but also in Mg alloys containing Al (e.g., AJ52) when the Sr/Al ratio is 0.318–0.361.

5.3.6 Intermetallics of Y and/or Nd

Mg–Nd/Y intermetallics (Fig. 5.16a) $Mg_{41}Nd_5$, $Mg_{24}Y_5$, β ($Mg_{14}Nd_2Y$), are found in alloys such as WE43, WE54. β_1 is seen in WE43 and β is in WE54.[80,81] Crystal structures of these phases are given in Table 5.2 and the TEM diffraction data of β is shown in Fig. 5.16b.

© Woodhead Publishing Limited, 2013

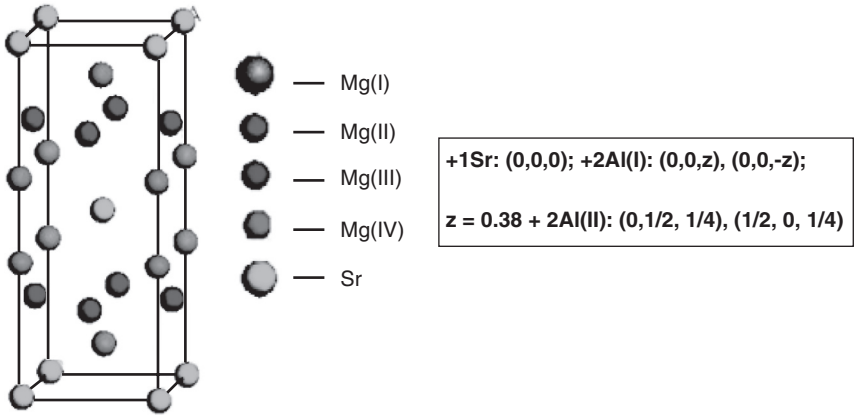

5.15 Model crystal unit cell of Al_4Sr.[79]

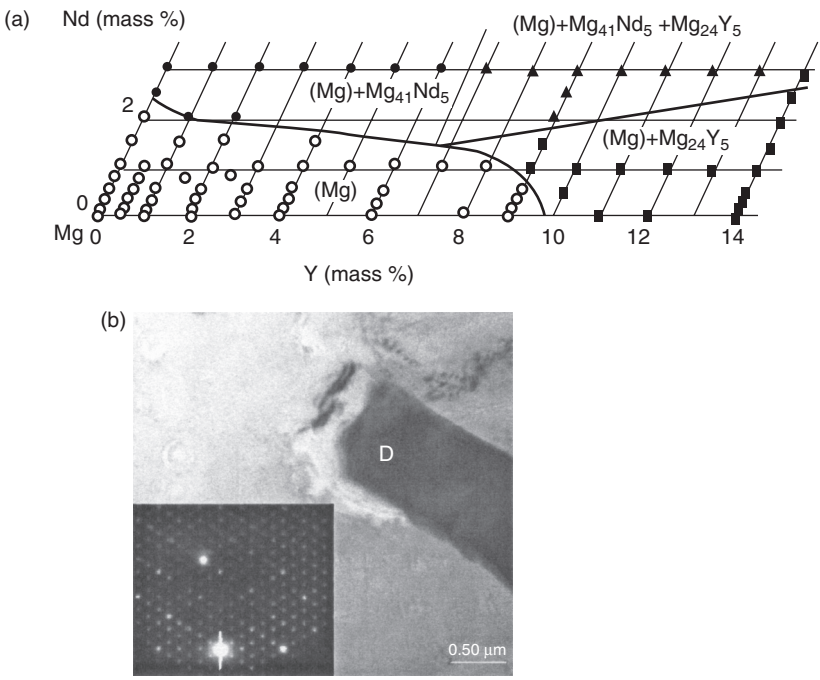

5.16 (a) Isothermal section of the Mg-Nd-Y phase diagram at 500°C.[80] (b) TEM image and SAED diffraction pattern of the β particle.[81] B// [-1–11].

© Woodhead Publishing Limited, 2013

5.4 The effects of second phases on the mechanical behavior of magnesium

Second phases that form in Mg alloys are usually intermetallic compounds, except for α-Mn which forms in Mg–Mn based systems and α-Li which forms in Mg–Li based alloys. Depending on their type and distribution, the second phases can contribute to strengthening and creep resistance. They can also play an important role in nucleating recrystallization and altering preferred orientation (texture) in wrought alloys.

5.4.1 Second-phase strengthening

Dispersion hardening (Orowan strengthening)

Non-coherent precipitates can provide strengthening by pinning dislocations if their size is small and they are closely spaced. The mechanism that causes the strengthening is the interaction of glide dislocations with the precipitates to increase the yield stress as

$$\tau_{\text{yield}} = \frac{(2\text{aGb})}{1+\tau_a}$$

where τ_{yield} = the yield strength of the alloy with second phases, τ_{a} = the yield strength of the matrix without precipitates,

(2aGb/l) = stress required to bow out dislocations between precipitates

In Mg casting alloys the second phases are non-coherent but they are coarse and are located at the grain boundaries since quite a number of the alloy systems (Mg–Al, Mg–Zn, Mg–Al–Zn, Mg–Al–RE, Mg–Al–Ca, Mg–Al–Sr) are eutectic. These phases strengthen grain boundaries but provide no Orowan strengthening inside the grains.

Precipitation hardening

Precipitation hardening, another mechanism of second-phase strengthening in alloys, occurs when the solid solubility decreases with decreasing temperature; this allows the solutionizing of as-cast second phases to be re-precipitated in a controlled fashion. When rapidly cooled from a homogeneous solid solution at high temperature, the alloy produces an unstable supersaturated solid solution which, upon aging for a sufficient time, may form fine and dispersed precipitates for further hardening. The precipitation may not go directly into the formation of the non-coherent equilibrium phase because of kinetic limitations and may instead go through a sequence

© Woodhead Publishing Limited, 2013

Table 5.3 Precipitation sequence in certain Mg alloys[30]

Alloys	Precipitation
Mg–Al	SSS[1)]-$Mg_{17}Al_{12}$
Mg–Zn (-Cu)	SSS-GP zones-$MgZn_2$ (rods, coherent)-$MgZn_2$ (disc, semicoherent)-Mg_2Zn_3 (triagonal, incoherent)
Mg–RE (Nd)	SSS-GP zones-Mg_3Nd (?[2)], hep)-Mg_3Nd (fcc, semicoherent)-$Mg_{14}Nd$ (incoherent)
Mg–Y–Nd	SSS-β' ($Mg_{12}NdY$)- β_1($Mg_{14}Nd_2Y$)
Mg–Ag–RE (Nd)	SSS-GP zones (coherent)-γ (?, coherent) SSS-GP zones (coherent)- β (?, semicoherent)-$Mg_{12}Nd_2Ag$ (incoherent)

SSS: supersaturated solid solution

of metastable intermediate precipitates. Chapter 4 provides a detailed discussion of precipitation hardening. Table 5.3 is provided here to show some of the possible precipitation sequences in certain Mg alloys.[30]

Age hardening requires some solid solubility, which occurs for Mg at around 12–15% atom size difference (Fig. 5.1). This region in Fig. 5.1 is also where there is some respectable solute strengthening. In the region where size factors are above 15% at around 20–40% (Cu, Ca, Si), where very limited solid solution is observed, there are also good opportunities for strength-enhancing elements, because here intermetallics and dispersoids of high melting point and high hardness are obtained for dispersion strengthening.

Dynamic precipitation

Dynamic precipitation is a term that can be used to describe precipitation which is thermally or stress-induced. Dynamic precipitation is common in cast alloys which are in non-equilibrium in the as-cast condition; upon thermal exposure, the alloy moves towards equilibrium, which may result in second-phase precipitation from the supersaturated matrix or from the supersaturated second phases. A well-known example is the precipitation of $Mg_{17}Al_{12}$ from the supersaturated Mg matrix in die-cast Mg–Al based alloys.[27] Dynamic precipitation has been observed in the AJ62 (Mg–6Al–2Sr) alloy that has been developed by Noranda in 2000–2, where Al–Mn particles precipitated out of the α-Mg matrix during elevated temperature heating.[6] A more recent example of dynamic precipitation has been reported in studies on Mg–Mn–Ce alloys with α-Mn nano-particles precipitating out of the supersaturated α-Mg and supersaturated eutectic $Mg_{12}Ce$ phase.[28,51,82]

© Woodhead Publishing Limited, 2013

5.4.2 Effects of second phases on creep

Mg alloy research focused on developing creep-resistant Mg casting alloys for automotive powertrain applications in the time period between 1991 and 2006. Hence, alloy design for creep resistance has become important. Second phases play a key role in determining the creep resistance of Mg alloys.

a. *Thermally stable intermetallic compounds at the grain boundaries* of the cast material may strengthen the alloy against grain boundary migration by providing obstacles to grain boundary motion) and against grain boundary diffusion (by increasing the atomic packing). Examples are Al_4Sr in Mg–Al–Sr alloys (AJ62). The thermal stability of the Al_4Sr phase is one of the key attributes of AJ62 in attaining its creep resistance.
b. On the other hand, grain boundary intermetallics that show thermal/*metallurgical instability* via coarsening or phase transformation exhibit local strain which causes grain boundary migration (GBM) or grain boundary diffusion (GBD) at elevated temperatures. There are numerous examples of this in Mg alloys, which results in loss of creep resistance: (i) the decomposition of $Al_{11}RE_3$ into Al_2RE and Al to form $Mg_{17}Al_{12}$ in AE42 above 150°C,[52] (ii) the decomposition of Mg_9Al_3Sr in AJ63 alloy,[6] (iii) the transformation of $\beta_1(Mg_{12}NdY)$ to $\beta(Mg_{14}Nd_2Y)$ in WE alloys at 300°C,[83] (iv) the transformation of age-hardening precipitates in Mg–Y–RE alloys.[83]
c. *Intradendritic precipitates*, when fine, closely and uniformly spaced, and in a large quantity, can be effective against the most common creep deformation process in Mg alloys under the service conditions of powertrain components, that is, dislocation climb. Such precipitates can be produced in the as-cast alloys by peritectic reactions or by precipitation hardening. In order to be effective, these precipitates need to successfully pin dislocations and maintain thermal stability at the creep temperatures. Most age-hardening precipitates lose their effectiveness against dislocation climb at temperatures where they are prone to coarsening and phase transformations. An important contribution to creep resistance comes from the fine dispersion of Mn_2Sc disc precipitates in Mg–Gd–Sc–Mn alloys – precipitates in overaged Mg–Gd–Nd–Zr alloys, and α Mn precipitates formed via precipitation from the α-Mg matrix upon temperature exposure in Mg–Mn alloys.[82–86]
d. Creep-induced dynamic precipitation of second phases can either impart or be detrimental to creep resistance. It can be said that the resistance of Mg alloys to dislocation climb can largely be attributed to the dynamic precipitation of fine particles during creep. In AJ62 alloy, the precipitation

© Woodhead Publishing Limited, 2013

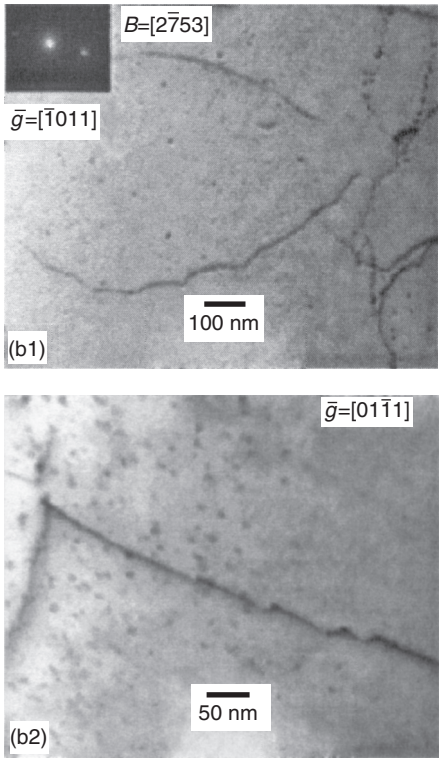

5.17 Effective dislocation pinning by Al–Mn precipitates in AJ alloys.[6]

of Al–Mn particles (Fig. 5.17) from the matrix leads to effective dislocation pinning.[6] In Mg–Ce–Mn alloys, the intradendritic co-precipitation of α-Mn with $Mg_{12}Ce$ slows down dislocation glide within the dendrites and delays the pile-up of dislocations at the intermetallic interface, preventing intermetallic cracking and the early onset of tertiary creep.[28,51,82] Alloys that are heat treatable can be used in solution heat-treated (T5) condition to allow for fine precipitation during creep. Gd and Y alloys with Mn and Sc in the T5 condition exhibit dynamic precipitation from the solid solution of stable Mg_5 Gd type phase (~2 μm in size) inside the grains during creep, which interact effectively with dislocations.[83–86]

e. *Interdendritic intermetallics* can also lead to the early onset of tertiary creep by cracking if the intradendritic and/or interdendritic region of the alloy is not able to prevent easy glide and strain accumulation at the matrix/intermetallic interface. Examples are the cracking of $Mg_{12}Ce$ interdendritic in Mg–Ce–Mn alloys when the dislocation pinning effect of α-Mn fine precipitates is lost leading to the formation of HDD zones at the matrix/intermetallic interface.[51]

© Woodhead Publishing Limited, 2013

5.4.3 Effects of second phases on the recrystallization of wrought Mg alloys

The second phases exert their influence on Mg alloy recrystallization in two ways: (i) they influence grain growth and (ii) they can nucleate new grains through a mechanism called particle-stimulated nucleation (PSN).

Second-phase interaction with grain growth

Fang *et al.*[87] studied the microstructures and mechanical properties of rolled AZ61 alloys containing different levels of Y (0–1.4%Y). Y refined the average grain size; Al_2Y second phase which had been finely broken during rolling was claimed to suppress grain growth. Mg–Li–Al–Zn–RE alloy (LAZ532–2RE), when extruded, recrystallized to a fine grain size[88] which was attributed to grain boundary pinning and to the retardation of grain growth by the fine Al_2Y precipitates. He *et al.*[89] observed grain refinement in the extruded/heat-treated (T6) structure of 1.3%Gd alloyed ZK60. The grain refining effect of Gd was attributed to grain boundary pinning by Mg-Zn-Gd phase particles.

Particle-stimulated nucleation

PSN is a mechanism whereby the recrystallization of the deformed metal is activated at the interface of second-phase particles. The important attributes of the second-phase particles in nucleating recrystallization are known to be optimal size and non-coherency, to ensure sufficient accumulation of dislocations to nucleate recrystallization.

The thermal stability of the precipitates is also of prime importance in maintaining the effectiveness of PSN at high temperatures. Competing mechanisms that occur at low temperatures (twinning, grain boundary bulging) and at high temperatures (non-basal slip) may overshadow PSN even when there are appropriate second phases.[90] The size of the distributed particles is also important. Clusters of particles, even when they are clusters of fine (<1 μm) particles, are known to be more effective than single particles.[91] Different alloys exhibiting PSN during recrystallization are presented in Table 5.4.

5.5 Alloying with surface-active elements

Surface-active elements are specific to a metal system and are those solutes that segregate to the surface because they decrease its surface energy. The surface could be liquid metal surface, solid surface, grain boundaries or the interface between the matrix and the second phase. In the case of liquid surfaces,

© Woodhead Publishing Limited, 2013

Table 5.4 PSN in different Mg alloys

Alloy	Precipitate	Deformation process	Effect	References
Mg + Mn	Mn particles	Hot compression	Matrix rotation at Mn particles	92
AZ41 + Mn,Ca	$Mg_{17}Al_{12}$, Al_8Mn_5, $A1_2Ca$	Hot compression	Large particles promote recrystallization. The geometry, size and distribution of the particles influence DRX	91, 93
AZ31	$Mg_{17}Al_{12}$ AlMn	Hot compression	Some evidence of PSN	94
AZ31	$Mg_{17}Al_{12}$, AlMn	Hot compression	PSN took place during hot deformation and was facilitated by the fragmentation of the $Mg_{17}Al_{l2}$	95
AZ31	$Mg_{17}Al_{12}$ AlMn	Twin roll casting (TRC)	PSN occurs due to high amount of second phase in the as-TRC metastable structure and contributes to texture weakening	96, 97
AZ31 + Sr	Al_4Sr	Extrusion	Al_4Sr stringers lead to PSN and texture weakening at 350°C but not at 250°C	98, 99
Mg–1Mn + Sr	$Mg_{17}Sr_2$, Sr_5Si_3	Rolled sheet	Stringers cause PSN and texture weakening	100, 101
Mg–1Zn + Sr	Sr–Si compounds (SrSi, Sr_5Si_3)	Rolled sheet	Stringers cause PSN and texture weakening	100
WE43	Mg–Nd. Mg–Y Mg–Nd–Y	Extrusion	Recrystallization at second-phase particles were observed	102
WE54	Mg–Nd, Mg–Y Mg–Nd–Y	Extrusion	PSN took place and has weakened the basal texture	103

© Woodhead Publishing Limited, 2013

Table 5.5 Wigner-Seitz radii, *rSW*, of selected elements (nm)

Al	Mg	Sr	Ca	Ce	Ni	Nd	Si	Sb	Sn	Fe	Se	Te	Mn	Li
0.15	0.18	0.19	0.21	0.20	0.14	0.20	0.16	0.11	0.19	0.14	0.19	0.21	0.14	0.17

solute segregation can influence the surface tension and alter the chemical activity (e.g., oxidation) or the evaporation[104] of the alloy melt. Yamauchi[105] has performed the calculations using electron density profiles for a number of binary substitutional solid solutions and has formulated the rule that the element having the larger Wigner-Seitz radius, r_{WS} (*lower* average electron density), segregates to the surface. It implies that the driving force for surface segregation is reduction in the surface energy of the segregated alloy. This was reconfirmed by Kiejna *et al*.[106,107] for binary alkali-metal alloys (e.g., Na–K, Na–Cs). In other systems, Sb, Sn and Se have a strong tendency to surface-segregate on Fe and Fe–Si alloys (Table 5.1). Sb and Sn can alter the texture and improve the electrical properties of silicon steels, and Se and Te are surface-active in molten Fe and decrease wettability.[108] Micro-levels of surface-active Nd, Pr, Ce, La in nickel alloys, and of Ca in tool steels, poisons the grain boundaries and disperses carbides within the grains.[109] Ce is also surface-active in Al.[110] According to Table 5.5, Sr, Ca Ce, Nd, Sn, Se and Te would be surface-active in Mg based on their larger r_{WS} than Mg. These elements would reduce the surface energy and the surface tension of Mg.

5.5.1 Surface tension

It has been observed[111] that a number of elements alter the surface tension of liquid Mg (Fig. 5.18). As noted, Sr has a significant effect wherein the surface tension continues to decrease with increasing Sr. The surface activity gives a good guideline for surface segregation, but exceptions have been observed: for example, Zn surface-segregates in Mg but has a lower r_{WS} than Mg.[17] Sb also reduces the surface tension despite the smaller r_{WS}. It can be predicted from Fig. 5.18 that Sr would increase interdendritic feeding, thereby minimizing or altering shrinkage microporosity during casting. In the gravity cast AZ91 Mg alloy, Sr removes from the bulk the microporosity that results from the solidification shrinkage during dendritic freezing (which is usually present in long-freezing-range alloys such as AZ91) and concentrates it into the hot spot;[113] in the high-pressure die-cast AZ91, a porosity reduction is also observed[112] resulting in an improvement in pressure tightness (Fig. 5.19).

The reduction in the surface tension, in this case (whereby solutes segregate to the surface) is accompanied by a decrease in the number of Mg atoms occupying the surface. This decreases the vapor pressure and increases the

© Woodhead Publishing Limited, 2013

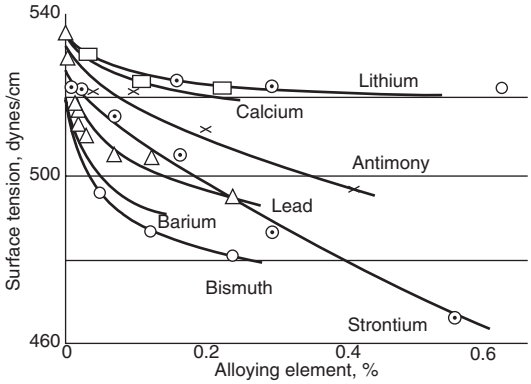

5.18 Effects of alloying elements on the surface tension of Mg.[111]

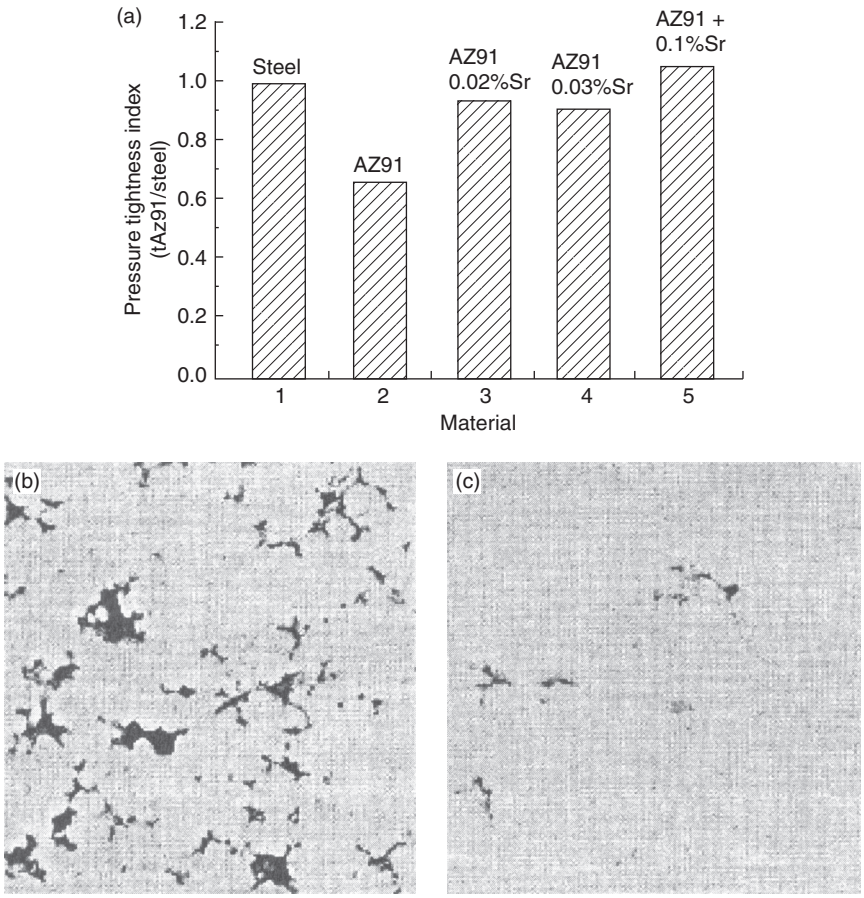

5.19 (a) Effect of Sr on the pressure tightness of die-cast AZ91D. Die-cast AZ91D (b) with no Sr; and (c) with 0.03 wt%Sr.[112]

© Woodhead Publishing Limited, 2013

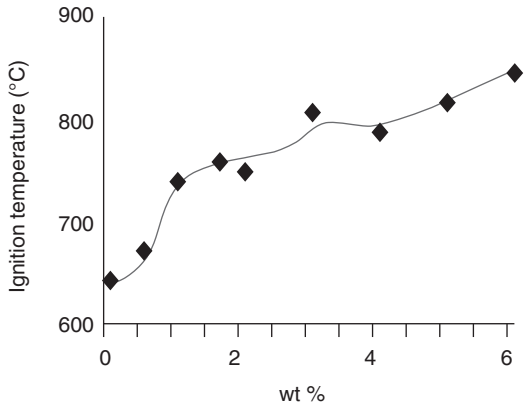

5.20 Ignition temperature vs. Sr.[114]

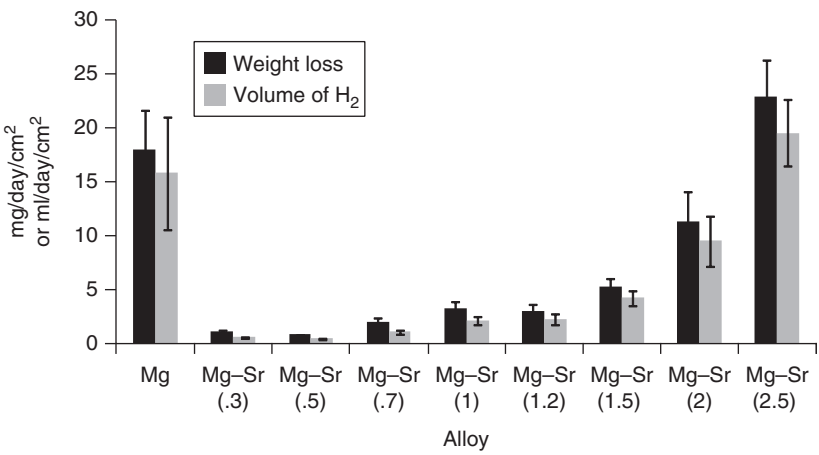

5.21 Biodegradation (weight loss; H_2 evolution) of Mg–Sr alloys in SBF (alloy compositions in wt%).[115]

ignition temperature of Mg. These effects have been observed in Mg–Sr, wherein the ignition temperature of the Mg–Sr alloy increases (Fig. 5.20) with increasing Sr content from 680°C at 0%Sr to 850°C at 6 wt%Sr.[114]

5.5.2 Bio-corrosion

Ca and Sr also improve (slow down) the bio-corrosion rate of Mg, paving the way for effective bio-absorbable cardiac and bone implants. Pekguleryuz and coworkers[115] have evaluated the biodegradation of Mg–Ca and Mg–Sr alloys; it was observed that compositions below 0.5% Sr and Mg-0.6%Ca

© Woodhead Publishing Limited, 2013

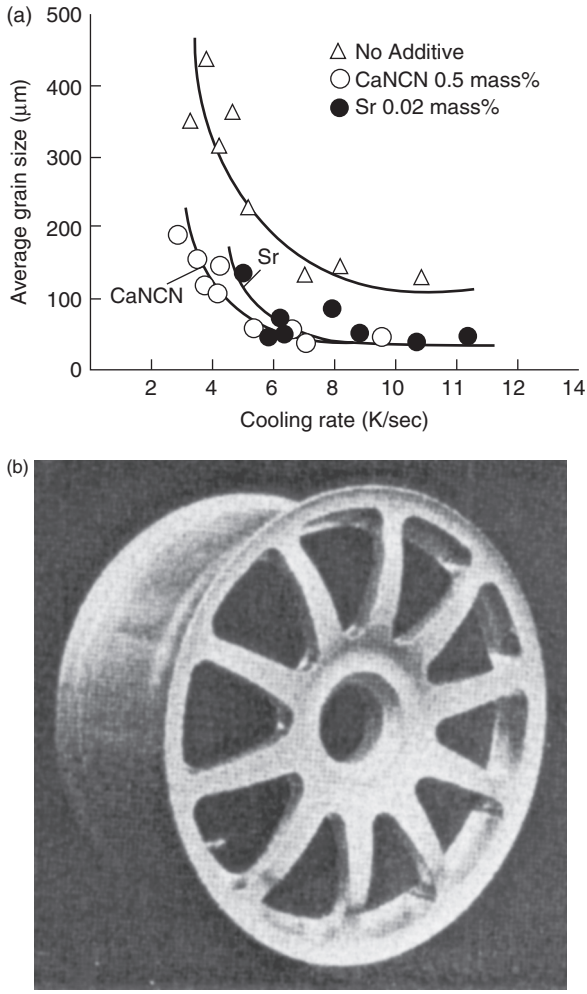

5.22 (a) The effect of Ca and Sr on grain refining; and (b) the Mazda wheel.[116]

show low rates of weight loss and hydrogen evolution (Fig. 5.21) in simulated body fluid (SBF). The improvement is related to the surface-active nature of Sr and Ca, which slows down the corrosion rate and improves the hydroxyapatite that forms on the surface.

5.5.3 Microstructural refinement

The criteria and rules governing the occurrence of fine grain boundary precipitates are not always clear. However, the selection of elements with a

© Woodhead Publishing Limited, 2013

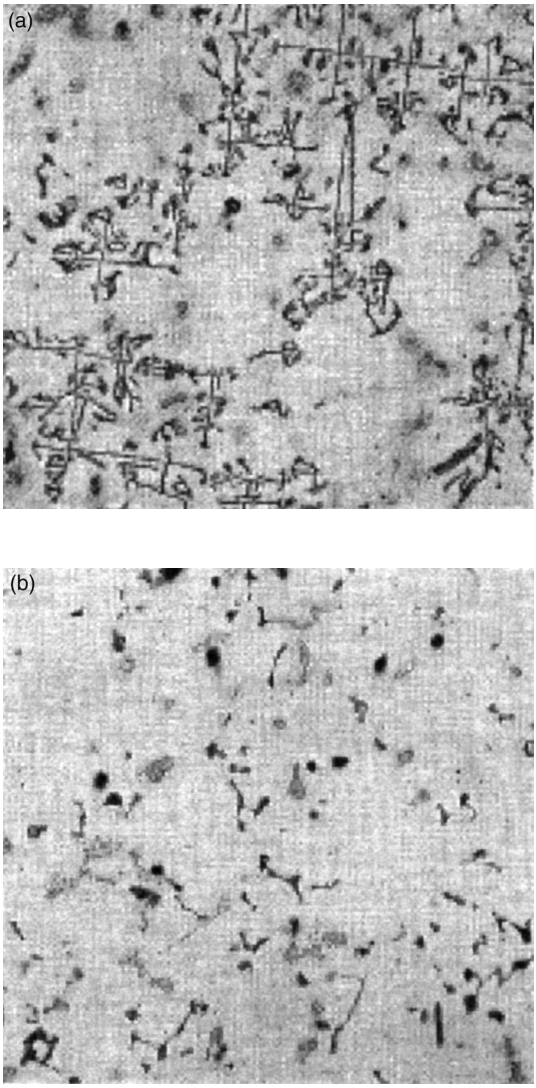

5.23 Microstructure of gravity cast (a) AS41 alloy with Chinese script Mg_2Si phase; (b) same alloy with 0.1 wt% Ca with refined Mg_2Si phase.[41]

probability of forming fine precipitates or refining existing phases can be facilitated by tapping into the knowledge base of other metal systems where these phenomena have occurred. Some of the elements, such as Ce, Ca or Sr, Ba and Sb, can be used in the microstructural design of many Mg alloys.

In Mg, the refining effect of Sr and Ca on the grain size and the $Mg_{17}Al_{12}$ phase in Mg–Al alloys had been first identified by Koubichek[111] in 1959.

© Woodhead Publishing Limited, 2013

Table 5.6 Mechanical properties of sandcast Ca-modified AS41 (parentheses give the sample size)[41]

Alloy	UTS (MPa)	YS (MPa)	Elongation (%)	Elastic modulus (GPa)	Mg_2Si morphology
AS41	152 ± 7 (14)	84 ± 3 (14)	1.9 ± 0.3 (9)	45 ± 3 (14)	Chinese script
AS41 + 0.06%Ca	155 ± 2 (16)	85 ± 2 (16)	4.5 ± 0.7 (15)	46 ± 2 (16)	Semi-dispersed
AS41 + 0.11%Ca	163 ± 7 (18)	85 ± 2 (18)	4.2 ± 0.7 (18)	49 ± 2 (18)	Dispersed
AZ91C	165	93	3.5	–	N/A

Comparing the Wiegner–Seitz ratio (Table 5.5), it can be seen that Sr and Ca would segregate to the surface or interfaces in Mg. This effect had not been explored for many years until Aliravci *et al*.[113] observed the grain refining effect of Sr in AZ91 (Mg–9Al–1Zn) alloy. This led to the use of Sr to grain-refine Mazda AZ80 forging wheels (Fig. 5.22).[116] In recent years more work has been carried out on the grain refining of Mg alloys via Sr.[117,118] Pekguleryuz *et al*.[41] used Ca in the 1990s to refine the Mg_2Si Chinese script morphology (Section 5.3.2) in the AS41 (Mg–4Al–1Si) alloy (Fig. 5.23) and a significant improvement in ductility of the gravity castings was obtained at 0.1%Ca additions (Table 5.6). In 2006, the Mg_2Si phase was refined by 0.1%Sr and Sb additions.[119,120]

5.6 Alloying elements and their effects

5.6.1 Al, Zn and Mn[8,26]

The most widely used alloys in this group are the AZ (Mg–Al–Zn) and AM (Mg–Al–Mn) series. Figure 5.24a illustrates the effects of Al and Zn on the strength and ductility of binary Mg alloys. The 3% Zn alloy is shown to be the most ductile, and the 9% Al alloy gives the maximum strength. Where a compromise needs to be made between strength and ductility, a binary 6% Al alloy (AM60, AZ61) offers acceptable strength, while a 5% Zn offers acceptable elongation. The combined effect of Al and Zn on Mg is not only on mechanical properties but also on castability (Fig. 5.24b). Al and Zn (up to 3%) improve the fluidity of Mg, making it castable. Al also influences corrosion resistance: Al decreases the corrosion resistance until ~8%, after which a reversal in behavior is seen.[121] For the AZ91 alloy where Al content ranges from 8.3% to 9.7%, great variations in corrosion resistance are inevitable. Tighter control of the Al limits may be a preferable measure in the future to avoid these variations.

© Woodhead Publishing Limited, 2013

Various problems related to molten metal handling and corrosion of these alloys due to heavy metal contamination have been solved over the last two decades. The most serious handicap with these alloys is poor high temperature strength, especially in cast parts. Their microstructure is characterized by $Mg_{17}Al_{12}$ (γ in the Al–Mg phase diagram, but also called β in the Mg alloy literature) intermetallic precipitates in a matrix of primary Mg. The β-precipitate has a cubic crystal structure incoherent with the HCP lattice of the matrix (Section 5.3.1). It exhibits covalent as well as metallic bonding and is prone to thermal instability.

5.6.2 Rare earth (RE) elements

REs impart both room and elevated temperature (200°C) strength to Mg. The strengthening is due to solid solution of the borderline sized RE atoms and second-phase hardening due to the $Mg_{12}X$ intermetallic (where X denotes RE element). The intermetallics (Table 5.2) have relatively low diffusivity (line compounds) at moderate temperatures and good matrix coherency.[122] Additional elements, such as Ag, may further improve the age-hardening response (such as in QE22 alloys). Die-casting alloy, AE44 has been utilized in the Corvette engine cradle. It takes advantage of the fluidity imparted by Al and the creep resistance imparted by REs. Al decreases somewhat the effect of REs due to the preferential formation of Al_2X which removes RE from solution. The alloy is costly but relatively easy to cast and has good creep properties. $Al_{11}RE$ is prone to phase transformation at moderate temperatures, making the alloys such as AE42 thermally unstable.

The major beneficial effect of REs on Mg is on creep strength up to 200–250°C. In Mg–Ce alloys it has been discovered that there is additional nucleation of a fine $Mg_{12}Ce$ precipitate at the grain boundaries during creep at 200–300°C, which is the decisive factor in improving the creep performance of Mg at 300°C by strengthening the grain boundaries. Furthermore, the additions that inhibit the coarsening of such fine precipitates contribute further to creep resistance. Mn further increases the creep strength of Mg–Ce alloys by restricting or altering the kinetics of the growth and altering the habit planes of $Mg_{12}Ce$ to achieve and maintain a fine dynamic precipitation.[51] The creep mechanism of REs can shed light on the development of creep-resistant Mg alloys. REs are surface-active in Mg and they can be used to modify and refine microstructural features, and for improving the oxidation and corrosion resistance. The beneficial effects of REs on the strength of Mg had been discovered as early as the 1930s and many commercial casting alloys suitable for gravity casting and some wrought alloys have been developed. Because of the higher cost associated with the RE alloys they have

© Woodhead Publishing Limited, 2013

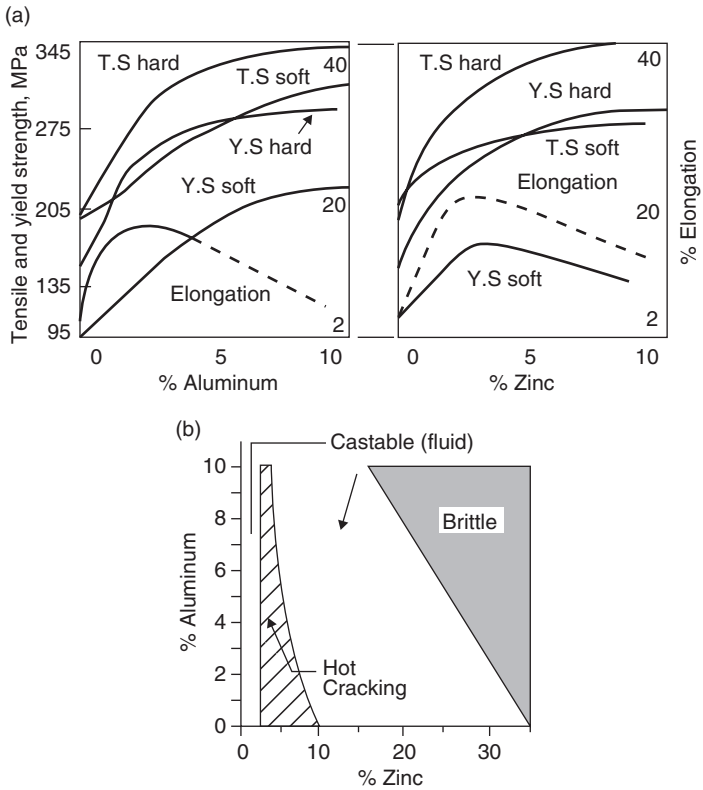

5.24 The effects of Al and Zn on (a) the mechanical properties of Mg and (b) castability.[8,26]

been mainly used for aerospace applications. A number of ternary and quaternary alloys have been commercialized, such as the ternary Mg–RE–Zr (EK30) and the quaternary alloys Mg–Zn–RE–Zr (ZE63, EZ33).

Selection of alternate lower cost solutes that produce similar intermetallic compounds in combination with solutes that stabilize them could be the key consideration for future work. However, most RE intermetallic compounds in Mg alloys have moderate melting points and most are subject to phase transformations, making the alloys metallurgically and thermally unstable for certain elevated temperature service. Other shortcomings are the high cost and the lack of worldwide supply of REs, posing a concern for high volume cost sensitive applications.

5.6.3 Alkaline earth elements

Alkaline earth elements Ba, Ca, Sr, like Mg, belong to Group II of the periodic table and exert effects similar to the REs when alloyed into Mg. Ba is

© Woodhead Publishing Limited, 2013

not recommended for use in commercial alloys since the storage of Ba as a raw material poses some safety problems.

Alkaline earths are surface-active and, like REs, improve the corrosion and oxidation resistance of Mg (including bio-corrosion resistance) and also refine the grain size and the size of the second phases.[111–120] They form intermetallic compounds with Mg and with Al in Mg–Al alloys,[55–72] which strengthen the grain boundaries and thereby increase creep resistance. These intermetallics are thermally more stable than the RE compounds: due to the negligible solubility of the alkaline earths in Mg at the elevated temperatures, they do not dissolve in the matrix or transform to other compounds by reacting with aluminum in Mg–Al alloys like some of the Al–RE intermetallics. The Sr compounds, due to their thermal stability, play a more effective role in PSN of recrystallization during rolling and extrusion than do the Mg–Re intermetallics at elevated temperatures.[10,70–78]

5.6.4 Group IV and group V elements[7]

Another area for further investigation is the effect of elements such as Sn, Sb and Bi on strength.[7] These elements form line compounds of high melting point. Because of the low ductility of the binary systems, they should be investigated in combination with elements that impart ductility such as Zn or Al. An important element addition to replace the REs partially, or to take the place of Ag, may be Sb. Sb has been used to produce creep-resistant solder alloys such as the 95/5 Sn/Sb.

The precipitates of the Ag containing alloys have not been completely determined yet but it is known that in the case of the Mg–Ag system, 'electron compounds' of simple lattice structures (BCC AgMg at an electron: atom ratio of 1.5 and HCP $AgMg_3$ at a ratio of 1.8) form.[8] These simple phases may more readily maintain coherency with the HCP Mg matrix.

Sb is also known to refine the grain size and the second phases in Mg alloys,[119] even though it is not predicted to be surface-active based on Wigner–Seitz radii (Table 5.5). The refining effect may be related to nucleant effects rather than to growth inhibiting effects related to surface activity.

5.7 Summary: magnesium alloy design to enhance properties

5.7.1 Strength and ductility

When the mechanical properties of a series of binary Mg alloys are examined under comparable conditions, it is seen that alloying elements fall into three main categories[7,8]

© Woodhead Publishing Limited, 2013

i. Those that increase both strength and ductility. These elements in order of effectiveness are:
   Al, Zn, Ca, Ag, Ce, Ga, Ni, Cu, Th (strength criteria)
   Th, Ga, Zn, Ag, Ce, Ca, Al, Ni, Cu (ductility criteria).
ii. Those which provide little strengthening, but increase ductility: Cd, Tl and Li.
iii. Those which may confer considerable strengthening but at the cost of ductility. These are: Sn, Pb, Bi and Sb.

Based on the above information, it is not surprising that most common alloy systems have been developed in the Mg–Al, Mg–Zn and Mg–Al–Zn systems.

5.7.2 Creep resistance in cast alloys[122]

Alloying elements exert their influence on creep through solute effect or second-phase formation.

i. REs and Y reduce GBD, pipe diffusion, and decrease primary creep rate. Ce produces Mg_{12} Ce or $Al_{11}Ce_3$, which are unstable at elevated temperatures, but Nd and Y produce interdendritic and intradendritic intermetallics, some of which are thermally stable.
ii. Sr produces the thermally stable Al4Sr against GBD and GBM in Mg–Al alloys. Sr also reduces Al solubility in Mg, leading to the dynamic precipitation of Al–Mn in Mg–Al–Sr (Mn) alloys.
iii. Mn produces fine intradendritic α-Mn phase which co-precipitates dynamically with fine $Mg_{12}Ce$ particles, refining its size and leading to effective dislocation pinning.[51,82]

5.7.3 Formability[123]

Since the main cause of low formability of Mg at room temperature (lack of at least five slip systems that activate) is its HCP crystal structure with a c/a of 1.624. Li additions, which influence the c/a (for Li < 2 wt%) or change the crystal structure to BCC(Li > 14 wt%), are perhaps the most potent alloying elements for improving the yield symmetry and the uniform deformation in Mg alloys. Li may, however, adversely affect strength; furthermore, alloying, melting and casting processes are very challenging.

A further difficulty in forming Mg wrought alloys is the preferred orientation (basal texture) that develops when Mg alloys are rolled or extruded. Alloying elements that have contributed to weakening of the strong basal texture in wrought Mg are RE elements, Y, and Sr.

© Woodhead Publishing Limited, 2013

Table 5.7 E_{corr} (V_{SCE}) for intermetallic phases and impurities in 0.1 M NaCl.[125]

	Mg_2Ca	Mg	$Mg_{24}Y_5$	$Mg_{12}La$	$Mg_{12}Nd$	Mg_2Si	$Mg_{12}Ce$	$Mg_{17}Al_{12}$	Mn	$MgZn_2$	Fe	Ni	Cu
E_{corr}	−1.75	−1.65	1.60	−1.60	−1.55	−1.54	−1.50	−1.35	−1.28	−1.03	−0.60	−0.22	−0.15

5.7.4 Corrosion resistance[124]

Magnesium has low corrosion resistance due to its highly negative corrosion potential of −2.37 V. It also ignites at ~680°C due to its high vapor pressure following surface oxidation which increases the local surface temperature very rapidly. Bulk magnesium, because of its high thermal conductivity, can dissipate the heat from the surface quickly; consequently it is difficult to ignite bulk magnesium, but chips will ignite rapidly.

Magnesium alloys are also susceptible to micro-galvanic corrosion which results from the difference between the corrosion potentials of the Mg matrix and the intermetallic second phases. Table 5.7 gives the corrosion potential (E_{corr}) of some of the second phases found in Mg alloys.

Alloying elements influence the corrosion behavior of Mg in various ways. Al improves the corrosion resistance up to a limit of ~8 wt% after which the corrosion resistance falls likely due to enhanced micro-galvanic corrosion.[121] Mn added to Mg–Al alloys removes the Fe impurity during molten state and settles it to the bottom of the crucible as sludge; when the solubility is reduced with the addition of Al, the separation of the Fe–Mn sludge compounds in the molten state becomes possible. Mn is not as effective in removing Fe from other Mg alloys, where it has some solid solubility and does not settle out in the molten state.

Surface-active elements, Ca, Sr and REs change the surface composition of the Mg alloy and modify the driving force for corrosion, and oxidation. Second phases that have corrosion potential quite different from Mg (Table 5.7), and impurities such as Fe, Cu and Ni, are detrimental to the corrosion resistance of Mg because they lead to micro-galvanic corrosion.

5.8 References

1. M.R. Stoudt, 'Magnesium: applications and advanced processing in the automotive industry', *JOM*, **60**(11), 2008, 56–56.
2. M. Easton, 'Magnesium alloy applications in automotive structures', *JOM* **60**(11), 2008, 57–62.
3. K. Johnson, 'Magnesium automotive applications,' *Adv. Mater. Proc.*, **160**(6), 2002, 62–65.
4. M. Pekguleryuz, E. Baril, P. Labelle, D. Argo, 'Creep resistant Mg-Al-Sr alloys', *J. Adv. Mater. Proc.*, **35**(3), 2003, 32–38.

© Woodhead Publishing Limited, 2013